Transactions of the 15th International Conference on
Structural Mechanics in Reactor Technology (SMiRT-15)
Seoul, Korea, August 15-20, 1999

Experiments and Constitutive Modelling for Uniaxial Ratchetting of 316 FR Steel at Room Temperature

Nobutada Ohno, Mohamed Abdel-Karim and Mamoru Mizuno

Nagoya University, Japan

ABSTRACT: This paper deals with experiments and constitutive modeling for uniaxial ratchetting of 316FR steel at room temperature. Cyclic tension tests, in which maximum strain increases every cycle by prescribed amounts of strain, are done systematically in addition to conventional monotonic, cyclic, and ratchetting tests. Thus hysteresis loop closure, cyclic hardening and viscoplasticity are discussed in the context of constitutive modeling for ratchetting. Then, the experiments are simulated by proposing a new kinematic hardening model which has two kinds of dynamic recovery terms. The model is featured with the capability of representing slight opening of stress-strain hysteresis loops robustly. The model is combined with a viscoplastic equation, and the resulting constitutive model is applied successfully to simulating the experiments.

INTRODUCTION

Strain accumulation induced by cyclic loading, i.e., ratchetting, is important in designing structural components. Uniaxial ratchetting, taking place under uniaxial cyclic loading with nonzero mean stress, can be most fundamental and has been studied in many works.

However, closure of stress-strain hysteresis loops have been scarcely studied in the context of constitutive modeling for ratchetting (Ohno et al., 1998). It is obvious that the closure is directly related with uniaxial ratchetting, because less ratchetting takes place under uniaxial cyclic loading if the closure is more perfect. Therefore, it is necessary to study the closure experimentally. It is also necessary to examine experimentally the effect of cyclic plastic and ratchetting strains on strain hardening. Although isotropic hardening is usually expressed in terms of accumulated plastic strain, it happens that accumulated plastic strain cannot be a good measure for isotropic hardening especially in ratchetting even if we consider only proportional cyclic loading (Ohno, 1982; Yoshida et al., 1989; Ohno et al., 1998).

In the present work, therefore, uniaxial ratchetting characteristics of 316FR steel at room temperature are studied experimentally with emphasis on the effects of hysteresis loop closure and viscoplasticity on ratchetting as well as the strain hardening in ratchetting. Then a new kinematic hardening model is formulated on the basis of the Armstrong and Frederick model (1966) and the Ohno and Wang model (1993, 1994) in the framework of strain hardening and dynamic recovery. The model is combined with a viscoplastic equation and applied successfully to simulating the experiments.

EXPERIMENTAL PROCEDURE

The specimens tested, which had the gauge sections of 8 mm in diameter and 30 mm in axial length (Fig. 1), were machined from a 316FR steel rolled sheet of 50 mm in thickness, so that the specimens had the axis oriented in the rolling direction of the sheet. The sheet had the chemical composition shown in Table 1. Each specimen was tested in the as-received state by using a 100-kN closed loop servohydraulic tension-compression testing machine with a digital controller. A clip-on extensometer of 25 mm gauge length was employed to measure the axial elongation. Either the axial elongation or the axial load was controlled.

EXPERIMENTAL RESULTS

In order to investigate hysteresis loop closure of 316FR steel, cyclic tension tests were performed in addition to conventional tests such as monotonic tension, cyclic straining between fixed strain limits, and uniaxial ratchetting (Table 2). Figure 2 illustrates the strain history in the cyclic tension tests. Six combinations of cyclic strain range $\Delta\varepsilon$ and maximum strain increment $\delta\varepsilon_{max}$ were chosen in the present work to examine their effects systematically; i.e., for each of three strain ranges of $\Delta\varepsilon$ =0.25, 0.4 and 0.8 percent, two tests of small and large increments of maximum strain, $\delta\varepsilon_{max}$ =0.01 and 0.1 (or 0.05) percent, were done at a constant strain rate of $\dot{\varepsilon} = 5\times10^{-3}$ percent/s. All the tests were done at room temperature.

Table 1 Chemical composition of 316FR steel (wt %)

C	Si	Mn	P	S	Ni	Cr	Mo	N
0.008	0.54	0.84	0.027	0.004	11.16	16.83	2.10	0.0754

Table 2 Loading conditions in experiments

Monotonic Tension	$\dot{\varepsilon} = 5\times10^{-1}$, 5×10^{-2}, 5×10^{-3}, 5×10^{-4}, 5×10^{-5}, 5×10^{-6}	
Cyclic Straining	$\dot{\varepsilon} = 5\times10^{-3}$	$\Delta\varepsilon$ = 0.25, 0.4, 0.8
Cyclic Tension $\dot{\varepsilon} = 5\times10^{-3}$	$\Delta\varepsilon$ = 0.25	$\delta\varepsilon_{max}$ = 0.01, 0.05
	$\Delta\varepsilon$ = 0.40	$\delta\varepsilon_{max}$ = 0.01, 0.10
	$\Delta\varepsilon$ = 0.80	$\delta\varepsilon_{max}$ = 0.01, 0.10
Ratchetting σ_{max} = 280	$\dot{\sigma}$ = 10	R = 0.0, −0.5, −0.75
	$\dot{\sigma}$ = 1	R = −0.75

stress (MPa), strain (%), time (s)

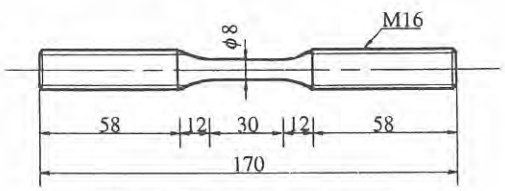

Fig. 1 Shape of specimens

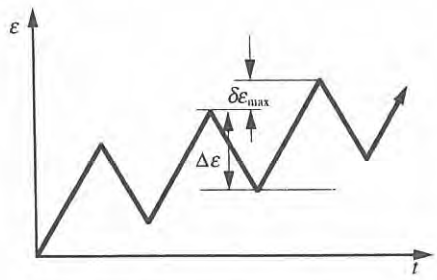

Fig. 2 Strain history in cyclic tension tests

Figures 3 (a) to (c) show stress and strain relations obtained in the cyclic tension tests, in which $\delta\varepsilon_{max}$ was prescribed to be large (i.e., $\delta\varepsilon_{max}$=0.05 or 0.1 percent). The dashed lines in the figures indicate the monotonic tensile relation at $\dot{\varepsilon} = 5\times10^{-3}$ percent/s. It is seen from the figures that the tests had the following features: In the tests of $\Delta\varepsilon$ =0.25 and 0.4 percent, the hysteresis loops closed almost perfectly, and the tensile peak points came to lie on the monotonic tensile curve; moreover, stress range varied little with the increase of the number of cycles, N. In the test of $\Delta\varepsilon$ =0.8 percent shown in Fig. 3(c), on the other hand, the tensile peak points had larger stresses than in the monotonic tension test, and stress range became larger noticeably with the increase of N. Therefore we can say that except for the effect of isotropic hardening the hysteresis loops closed almost perfectly in the three tests, and that isotropic hardening was negligible in the tests of $\Delta\varepsilon$ =0.25 and 0.4 percent but noticeable in the test of $\Delta\varepsilon$ =0.8 percent.

The same features were observed in the other cyclic tension tests shown in Figs. 4(a) to (c), in which the increase of maximum strain was much smaller, i.e., $\delta\varepsilon_{max}$=0.01 percent. However, taking a close look at the figures, we can see another feature: Let us pay attention to the cyclic tensile peak curves formed by linking the tensile peak points in the cyclic tension tests (Figs. 5(a) and (b)). It is then seen that the cyclic tensile peak curves in the tests of $\delta\varepsilon_{max}$=0.1 or 0.05 percent were almost the same as the monotonic tensile curve (Fig. 5(a)); on the other hand, the cyclic tensile peak curves of $\delta\varepsilon_{max}$=0.01 percent after saturation of cyclic hardening, which was significant in the test of $\Delta\varepsilon$ =0.8 percent, had smaller increase of stress than the monotonic tensile curve (Fig. 5(b)). It is moreover seen that this smaller increase of tensile peak stress occurred more noticeably when $\Delta\varepsilon$ was larger in the tests of $\delta\varepsilon_{max}$=0.01 percent (Fig. 5(b)). It is then suggested that the hysteresis loops in the cyclic tension tests had slight opening after saturation of cyclic hardening as a consequence of cyclic relaxation of mean stress.

Figure 6 depicts the changes of stress range $\Delta\sigma$ measured in the cyclic tension tests mentioned above. From the figure we see again negligible isotropic hardening in the cyclic tension tests of $\Delta\varepsilon$ =0.25 and 0.4 percent in contrast to noticeable isotropic hardening in the test of $\Delta\varepsilon$ =0.8 percent. This feature of isotropic hardening was observed under cyclic straining between fixed strain limits, as shown by the solid lines in the figure.

Now we discuss uniaxial ratchetting tests. The tests were done for four sets of stress ratio R and stress rate $\dot{\sigma}$ by prescribing maximum stress σ_{max} to be 280 MPa (Table 2). Here and from now on R denotes the stress ratio of minimum σ_{min} to maximum σ_{max}. The ratchetting tests were continued for 100 cycles. The stress-strain curves recorded in the

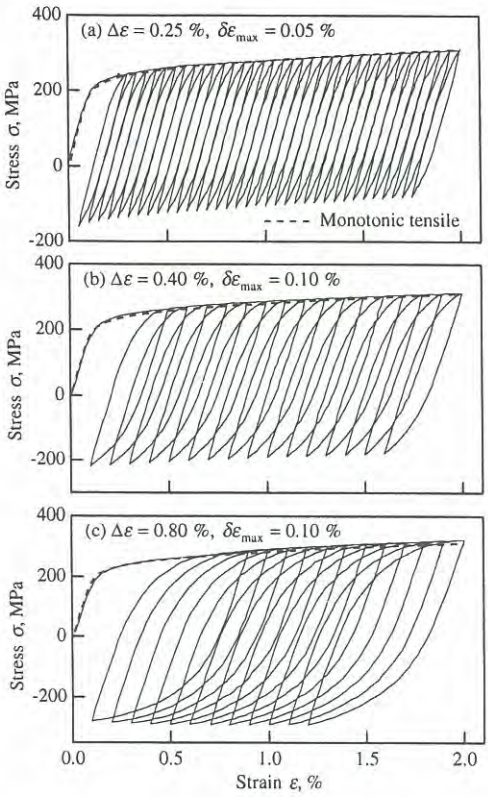

Fig. 3 Stress versus strain relations in cyclic tension tests with large increment of maximum strain δ_{max}

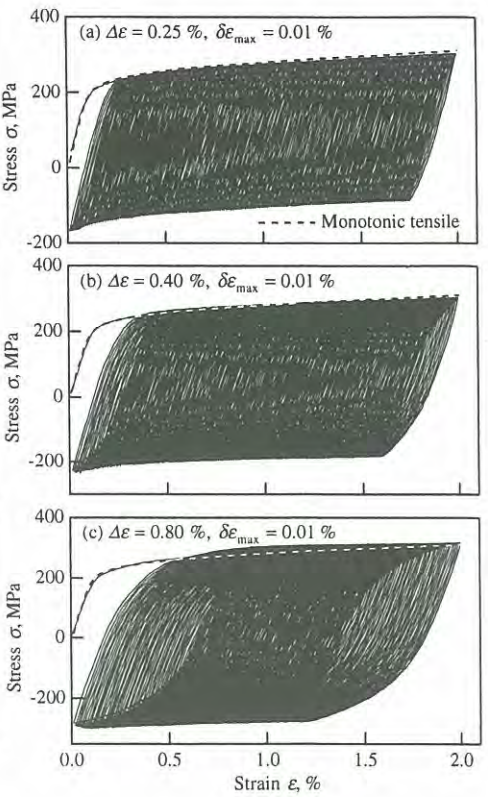

Fig. 4 Stress versus strain relations in cyclic tension tests with small increment of maximum strain δ_{max}

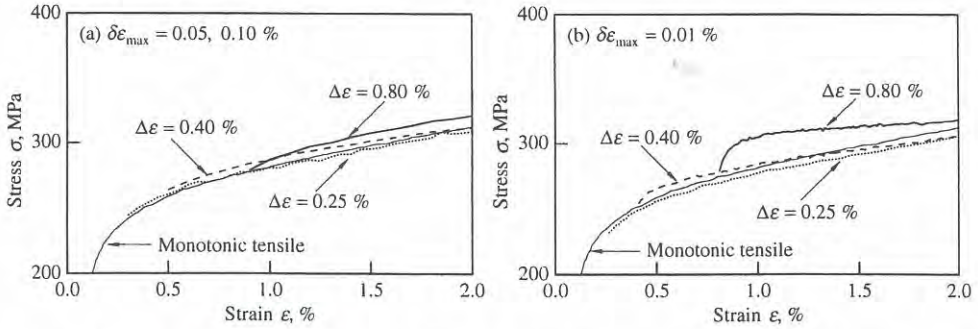

Fig. 5 Change of tensile peak stress in cyclic tension tests in comparison with stress change in monotonic tension test at $\dot{\varepsilon} = 5 \times 10^{-3}$ %/s

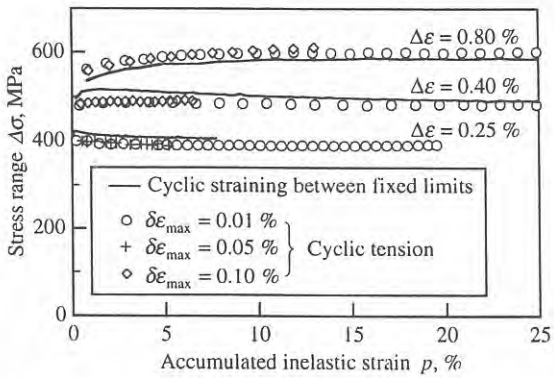

Fig. 6 Variation of stress range $\Delta\sigma$ as a function of accumulated inelastic strain p; cyclic straining between fixed limits (——) and cyclic tension (○, +, ◇)

uniaxial ratchetting tests are shown in Figs. 7(a) to (d). As seen from the figures, ratchetting proceeded without resulting in shaking down under the four loading conditions examined in the present work. The effect of $\dot{\sigma}$ or viscoplasticity was marked in the tests: Larger ratchetting took place in the test at $\dot{\sigma}=1$ MPa/s than in the other three tests, in which $\dot{\sigma}=10$ MPa/s. We remember that austenitic stainless steels exhibit viscoplasticity markedly at room temperature (Krempl, 1979; Kujawski et al., 1980). The effect of R, on the other hand, was not so significant: The three tests of $R=0$, -0.5 and -0.75 at $\dot{\sigma}=10$ MPa/s had nearly the same amount of ratchetting (Fig. 8), as was observed on 304 stainless steel at room temperature by Yoshida (1990).

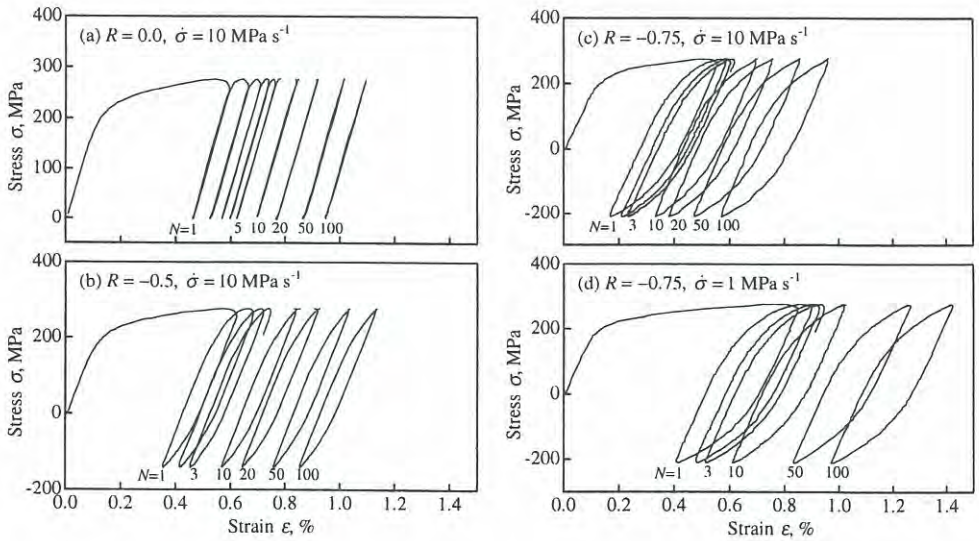

Fig. 7 Stress versus strain relations in ratchetting tests

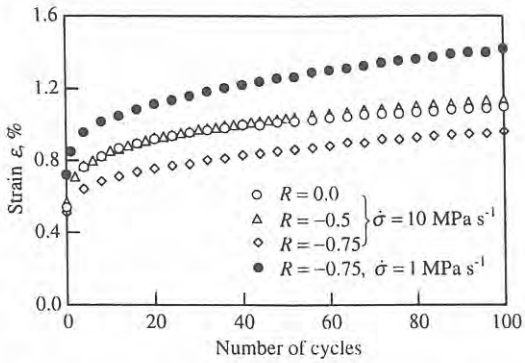

Fig. 8 Increase of tensile peak strain in ratchetting tests

Therefore, we can say that the slight opening of stress-strain hysteresis loops in cooperation with viscoplasticity can result in noticeable ratchetting under uniaxial cyclic stressing, suggesting the necessity of a constitutive model which can represent slight opening of hysteresis loops and viscoplasticity. We can also say that isotropic or cyclic hardening hardly develops if strain range is relatively small under cyclic straining, so that kinematic hardening governs almost strain hardening in ratchetting if stress range is not large.

CONSTITUTIVE RELATIONS

We assume that strain $\boldsymbol{\varepsilon}$ is divided additively into elastic part $\boldsymbol{\varepsilon}^e$ and inelastic part $\boldsymbol{\varepsilon}^p$,

$$\boldsymbol{\varepsilon} = \boldsymbol{\varepsilon}^e + \boldsymbol{\varepsilon}^p, \tag{1}$$

and that the elastic part obeys Hooke's law

$$\boldsymbol{\varepsilon}^e = \frac{1+\nu}{E}\boldsymbol{\sigma} - \frac{\nu}{E}(\mathrm{tr}\,\boldsymbol{\sigma})\boldsymbol{I}, \tag{2}$$

where E and ν indicate elastic constants, $\boldsymbol{\sigma}$ and $\boldsymbol{I}$ stress tensor and the unit tensor of rank two, respectively, and tr the trace. For the inelastic part, we employ a viscoplastic equation with back stress,

$$\dot{\boldsymbol{\varepsilon}}^p = \frac{3}{2} f(\sigma_{eff}) \frac{\boldsymbol{s}-\boldsymbol{a}}{\sigma_{eff}}, \tag{3}$$

where $\boldsymbol{s}$ and $\boldsymbol{a}$ indicate the deviatoric parts of stress $\boldsymbol{\sigma}$ and back stress $\boldsymbol{\alpha}$, respectively, and $f(\sigma_{eff})$ represents a material function of effective stress σ_{eff} defined as

$$\sigma_{eff} = \left[\frac{3}{2}(\boldsymbol{s}-\boldsymbol{a}):(\boldsymbol{s}-\boldsymbol{a})\right]^{1/2}. \tag{4}$$

Here and from now on $(\dot{})$ denotes the differentiation with respect to time t, $(:)$ the inner product between second rank tensors, and $<>$ Macauley's bracket, i.e., $<x> = (x+|x|)/2$.

It is noticed that isotropic hardening is ignored since isotropic hardening developed little in the ratchetting experiments.

We assume further that back stress consists of M parts as follows (Chaboche and Rousselier, 1983):

$$\boldsymbol{a} = \sum_{i=1}^{M} \boldsymbol{a}_i . \tag{5}$$

In order to express the change of $\boldsymbol{a}_i$, let us consider a combination of the Armstrong and Frederick model (1966) and the first version of the Ohno and Wang model (1993, 1994). The two models have a difference with respect to the dynamic recovery of $\boldsymbol{a}_i$. In the Armstrong and Frederick model, the dynamic recovery of $\boldsymbol{a}_i$ operates at all times in proportion to $\boldsymbol{a}_i$ and accumulating inelastic rate

$$\dot{p} = \left(\frac{2}{3} \dot{\boldsymbol{\varepsilon}}^p : \dot{\boldsymbol{\varepsilon}}^p \right)^{1/2} . \tag{6}$$

In the first version of the Ohno and Wang model, on the other hand, the dynamic recovery of $\boldsymbol{a}_i$ is assumed to take place only in a critical state, which is taken to be a hypersphere of radius r_i in the space of $\boldsymbol{a}_i$ such as

$$f_i = \frac{3}{2} \boldsymbol{a}_i : \boldsymbol{a}_i - r_i^2 = 0 . \tag{7}$$

Let us assume the two kinds of dynamic recovery terms mentioned above. Then, with Heaviside's step function H and Macauley's bracket $< >$, the evolution equation of $\boldsymbol{a}_i$ can be expressed as

$$\dot{\boldsymbol{a}}_i = \zeta_i \left[\frac{2}{3} r_i \dot{\boldsymbol{\varepsilon}}^p - \mu_i \boldsymbol{a}_i \dot{p} - H(f_i) \left\langle \overset{\circ}{\boldsymbol{\varepsilon}}_i^p : \frac{\boldsymbol{a}_i}{r_i} \right\rangle \boldsymbol{a}_i \right], \tag{8}$$

where ζ_i and μ_i are material parameters, and $\overset{\circ}{\boldsymbol{\varepsilon}}_i^p$ is defined in the following form to satisfy the consistency condition $\dot{f}_i = 0$:

$$\overset{\circ}{\boldsymbol{\varepsilon}}_i^p = \dot{\boldsymbol{\varepsilon}}^p - \frac{3}{2} \mu_i \frac{\boldsymbol{a}_i}{r_i} \dot{p} . \tag{9}$$

The second and third terms in the right hand side in Eq. (8) express the dynamic recovery of $\boldsymbol{a}_i$ based on the Armstrong and Frederick model and the Ohno and Wang model, respectively, whereas the first term is responsible for strain hardening.

It is readily seen that when $\mu_i = 0$ Eq. (8) reduces to the following equation, which is the first version of the Ohno and Wang model:

$$\dot{\boldsymbol{a}}_i = \zeta_i \left[\frac{2}{3} r_i \dot{\boldsymbol{\varepsilon}}^p - H(f_i) \left\langle \dot{\boldsymbol{\varepsilon}}^p : \frac{\boldsymbol{a}_i}{r_i} \right\rangle \boldsymbol{a}_i \right]. \tag{10}$$

On the other hand, when $\mu_i = 1$, it can be shown that Eq. (8) becomes the Armstrong and

Frederick model

$$\dot{a}_i = \zeta_i\left(\frac{2}{3} r_i \dot{\varepsilon}^p - a_i \dot{p}\right). \tag{11}$$

DETERMINATION OF MATERIAL PARAMETERS

The material parameters in the model, except μ_i, were determined on the basis of the uniaxial monotonic tensile experiments at different strain rates shown in Fig. 9. The material constants obtained are given in Table 3. The solid lines in Fig. 9 depict the tensile stress versus strain relations computed with $\mu_i = 0$. The material parameter μ_i, which was not determined from the tensile experiments, will be used to discuss the effect of hysteresis loop opening on the simulation of ratchetting and cyclic tension tests in the following section. It is worthwhile to point out here that the parameter μ_i has little influence on the uniaxial tensile behavior if $\mu_i < 0.5$, as shown in a specific case of $\dot{\varepsilon} = 5\times10^{-3}$ percent/s in Fig. 10.

Table 3 Viscoplastic function and material parameters

Elastic	$E = 1.96\times10^5$, $\nu = 0.3$	
Viscoplastic	$f(\sigma_{eff}) = 2.48\times10^{-10}\sinh\left\langle\frac{\sigma_{eff} - 75.0}{6.20}\right\rangle$	
Kinematic Hardening ($M = 10$)	$\zeta_1 = 1.00\times10^4$, $r_1 = 10.0$	$\zeta_2 = 5.00\times10^3$, $r_2 = 14.0$
	$\zeta_3 = 2.50\times10^3$, $r_3 = 17.3$	$\zeta_4 = 1.00\times10^3$, $r_4 = 22.0$
	$\zeta_5 = 4.00\times10^2$, $r_5 = 20.6$	$\zeta_6 = 1.84\times10^2$, $r_6 = 14.7$
	$\zeta_7 = 1.00\times10^2$, $r_7 = 6.40$	$\zeta_8 = 5.00\times10$, $r_8 = 10.0$
	$\zeta_9 = 3.33\times10$, $r_9 = 9.00$	$\zeta_{10} = 2.50\times10$, $r_{10} = 80.0$

stress (MPa), strain (mm/mm), time (s).

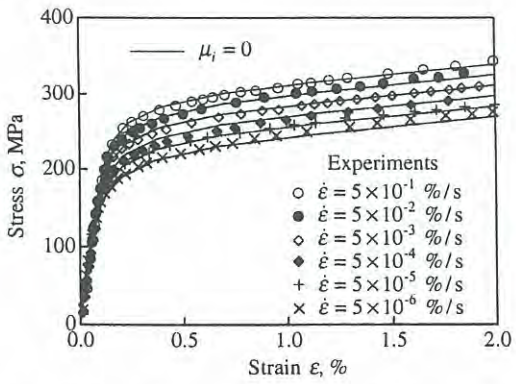

Fig.9 Uniaxial tensile stress-strain curves at constant strain rates

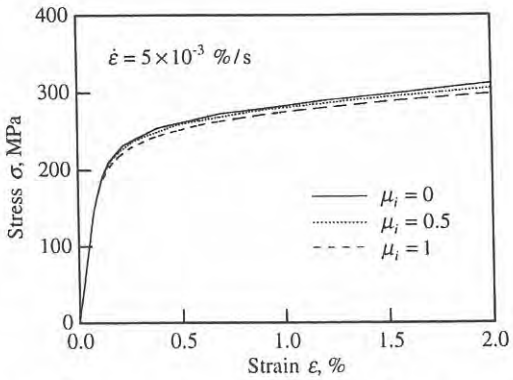

Fig.10 Influence of parameter μ_i on uniaxial tensile curve at $\dot{\varepsilon} = 5\times10^{-3}$ %/s

RESULTS OF SIMULATION

First let us deal with the ratchetting tests. Figures 11(a) to (d) compare the ratchetting experiments and the result of simulation obtained with the present constitutive model. The results of simulation are given with respect to four values of μ_i in each figure.

To begin with, we discuss the simulation obtained with $\mu_i = 0$. This choice of μ_i renders the α versus ε^p hysteresis loops closed perfectly, bringing in only the effect of viscoplasticity in simulating uniaxial ratchetting. As seen from Figs. 11(a) to (d), the present model with $\mu_i = 0$ simulates well the experiment of $R = 0$ but underestimates the other three experiments of R=-0.5 and -0.75. In other words, viscoplasticity accounts well for the

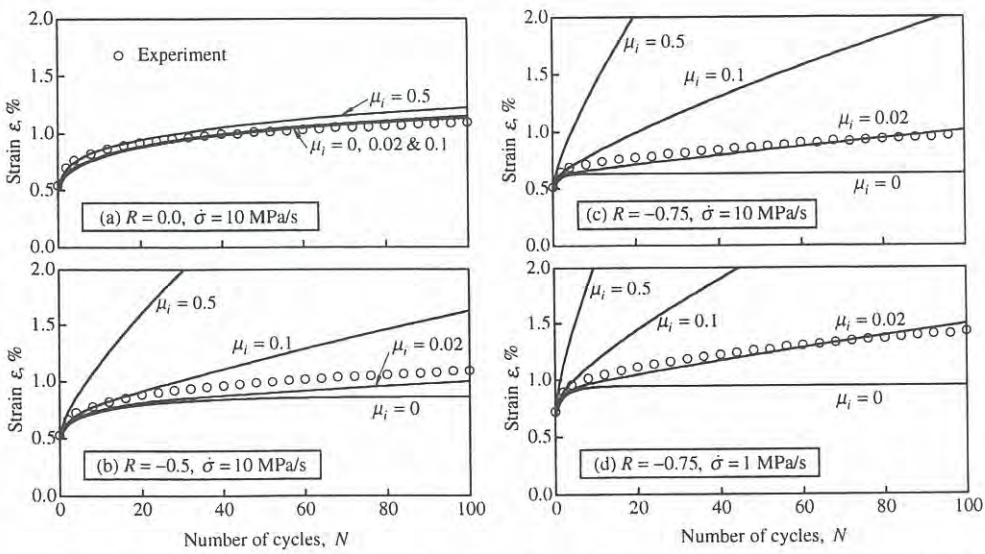

Fig.11 Increase of tensile peak strain under four stress cycling conditions (σ_{max} =280 MPa)

increase of strain under zero to tension cyclic loading, but only viscoplasticity is insufficient for predicting the experiments of R=-0.5 and -0.75. It is hysteresis loop opening that can be substantial more or less in uniaxial ratchetting of $R < 0$, in which reverse loading takes place. It is therefore necessary to consider hysteresis loop opening as well as viscoplasticity for simulating uniaxial ratchetting of 316FR steel at room temperature.

Here let us point out that if $\mu_i = 0$ ratchetting stops eventually under stress cycling of R=-0.5 and -0.75 (Figs. 11(b) to (d)). This is because Eqs. (2) and (8) with $\mu_i = 0$ make mean back stress grow monotonically with the increase of mean inelastic strain in ratchetting; then, as mean back stress becomes large, the stress versus strain hysteresis loops get symmetrized to have the same shapes in tension and compression sides, resulting in no further development of ratchetting due to viscoplasticity.

We are now in a position to discuss the effect of hysteresis loop opening, for which the parameter μ_i is responsible. As seen from Figs. 11(b) to (d), a larger value of μ_i gives more significant ratchetting under stress cycling of R=-0.5 and -0.75 though μ_i has little influence under zero to tension cyclic loading. It is emphasized that all the experiments examined are simulated well if $\mu_i = 0.02$. This value of μ_i is so small that the hysteresis loops can be opened only slightly to cause very slow ratchetting except for the effect of viscoplasticity. This is in accordance with the experimental fact that strain increased only by about 0.002 to 0.003 percent per cycle in the steady state when R=-0.5 and -0.75 (Figs. 11(b) to (d)). We have thus ascertained that ratchetting under stress cycling of $R < 0$ is driven by both viscoplasticity and slight opening of hysteresis loops.

Let us compare the results of simulation of $\mu_i = 0$ and $\mu_i = 0.02$ shown in Figs. 11(b) to (d). They start to deviate from each other after about twenty and five cycles when R=-0.5 and -0.75, respectively. Since only the effect of viscoplasticity is incorporated if $\mu_i = 0$, it is concluded that in the experiments of R=-0.5 and -0.75 viscoplasticity was effective in ratchetting in such early cycles whereas slight opening of hysteresis loops became influential as ratchetting proceeds, as was deduced experimentally.

Now let us consider the cyclic tension tests. Figures 12(a) to (c) illustrate the simulation of cyclic tension of large increments of maximum strain. The simulation is given only with respect to $\mu_i = 0.02$, which enabled us to simulate the ratchetting experiments best. As seen from the figures, the model with $\mu_i = 0.02$ represents the almost perfect closure of hysteresis loops, which was a characteristic observed in the experiments. The model thus simulates successfully the experiments except for the effect of isotropic hardening, which does not matter in the case of small strain ranges.

By showing the results of simulation with respect to three values of μ_i in comparison with the experiments, let us discuss the effect of hysteresis loop opening on the cyclic tension tests. Here we consider the case of $\Delta\varepsilon$ = 0.4 and $\delta\varepsilon_{max}$ = 0.01 percent (Figs. 13(a) to (c)). Let us start with the simulation obtained with $\mu_i = 0$. In this case, the model provides the complete closure of stress strain hysteresis loops, i. e., no cyclic relaxation of mean stress, and consequently the tensile peak points come to lie exactly on the monotonic tensile curve indicated by the dotted line (Fig. 13(a)). On the other hand, when $\mu_i = 0.02$, the model simulates slight cyclic relaxation of mean stress as in the experiment, so that smaller increase of tensile peak stress than in the monotonic tension test is expressed (Fig. 13(b)). When $\mu_i = 0.5$, cyclic relaxation of mean stress is too large to simulate properly the experiment, as shown in Fig. 13(c).

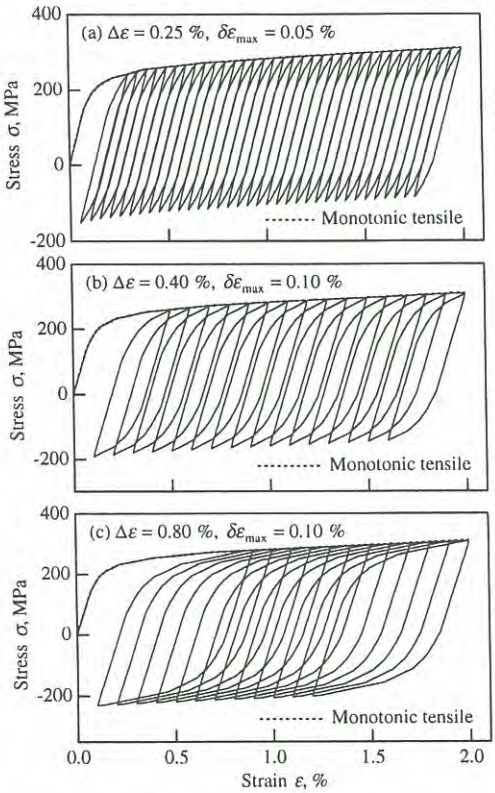

Fig. 12 Simulation of cyclic tension tests with large increments of maximum strain (μ_i=0.02)

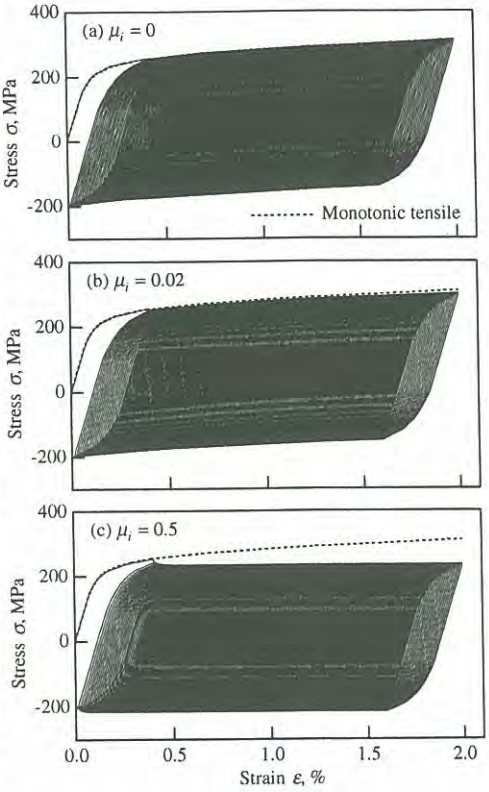

Fig. 13 Influence of parameter μ_i on the simulation of cyclic tension test under the condition of $\Delta\varepsilon$ =0.4 and $\delta\varepsilon_{max}$= 0.01 %

CONCLUSIONS

In the present work, uniaxial ratchetting characteristics of 316FR steel at room temperature were studied experimentally by performing cyclic tension tests as well as conventional tests such as monotonic tension, cyclic straining, and ratchetting tests. Then, a new kinematic hardening model capable of representing slight opening of hysteresis loops robustly was developed and combined with a viscoplastic equation in order to simulate the experiments. Main results can be summarized as follows:

(1) The hysteresis loops of stress and strain have slight opening, which in cooperation with the viscoplasticity induces uniaxial ratchetting of the material.

(2) Neither accumulated inelastic strain nor maximum inelastic strain induces isotropic or cyclic hardening markedly if strain range is small; in other words, only kinematic hardening is likely to govern strain hardening at any strain if strain range is small.

(3) A new kinematic hardening model capable of representing slight opening of stress-strain hysteresis loops was developed. The model was then combined with a viscoplastic equation with back stress, and the resulting constitutive model was applied successfully to simulating the ratchetting experiments of 316FR steel at room temperature

(4) Viscoplasticity and very slight opening of stress-strain hysteresis loops are responsible for the uniaxial ratchetting in early and subsequent cycles, respectively, when stress ratio is negative. For the uniaxial ratchetting under zero to tension cyclic loading, on the other hand, only viscoplasticity is the driving force.

REFERENCES

1. Armstrong, P. J. and Frederick, C. O., "A mathematical representation of the multiaxial bauschinger effect," *CEGB Report RD/B/N731, Berkeley Nuclear Laboratories*, Berkeley, UK, 1966.
2. Chaboche, J. L. and Rousselier, G., "On the plastic and viscoplastic constitutive equations, Part I: rules developed with internal variable concept, Part II: application of internal variable concepts to the 316 stainless steel," *ASME J. Pressure Vessel Tech.*, Vol. 105, 1983, pp. 153-164.
3. Krempl, E., "An experimental study of room-temperature rate-sensitivity, creep and relaxation of AISI type 304 stainless steel," *J. Mech. Phys. Solids*, Vol. 27, 1979, pp. 363-375.
4. Kujawski, D., Kallianpur, V. and Krempl, E., "An experimental study of uniaxial creep, cyclic creep and relaxation of AISI type 304 stainless steel at room temperature," *J. Mech. Phys. Solids*, Vol. 28, 1980, pp. 129-148.
5. Ohno, N., "A constitutive model of cyclic plasticity with a nonhardening strain region," *ASME J. Appl. Mech.*, Vol. 49, 1982, pp. 721-727.
6. Ohno, N. and Wang, J.-D., "Kinematic hardening rules with critical state of dynamic recovery, Part I: formulation and basic features for ratchetting behavior," *Int. J. Plasticity*, Vol. 9, 1993, pp. 375-390.
7. Ohno, N., Wang, J.-D., "Kinematic hardening rules for simulation of ratchetting behavior," *Eur. J. Mech., A/Solids*, Vol. 13, 1994, 519-531.
8. Ohno, N., Abdel-Karim, M., Kobayashi, M. and Igari, T., "Ratchetting characteristics of 316FR steel at high temperature, Part I: strain-controlled ratchetting experiments and simulations," *Int. J. Plasticity*, Vol. 14, 1998, pp. 355-372.
9. Yoshida, F., Kondo, J. and Kikuchi, Y., "Visco-plastic behavior of stainless steel SUS 304 under cyclic loading at room temperature," *Trans. JSME*, Ser. A, Vol. 54, 1988, pp. 1151-1157, (in Japanese).
10. Yoshida, F., "Uniaxial and biaxial creep-ratchetting behavior of SUS304 stainless steel at room temperature," *Int. J. Pressure Vessels and Piping*, Vol. 44, 1990, pp. 207-223.